Angewandte Chemie International Edition

Angewandte International Edition Chemie

How to cite: *Angew. Chem. Int. Ed.* **2026**, e8622158
doi.org/10.1002/anie.8622158

RESEARCH ARTICLE

A Rigid Molecular Triangle as an Ultrafast and Highly Selective Transmembrane Li^+ Channel

Mingju Luo[1] | Si-Dan Guo[2] | Junhao Zhang[1] | Wenju Chang[1] | Dong-Sheng Guo[3] | Yu-Wu Zhong[4] | Kang Cai[2] | Jie Shen[1] | Huaqiang Zeng[1]

[1]Fujian Provincial Key Laboratory of Molecular Synthesis and Functional Discovery and College of Chemistry, Fuzhou University, Fuzhou, China | [2]College of Chemistry, Nankai University, Tianjin, China | [3]College of Chemistry, State Key Laboratory of Medicinal Chemical Biology, Key Laboratory of Functional Polymer Materials (Ministry of Education), Frontiers Science Center For New Organic Matter, Collaborative Innovation Center of Chemical Science and Engineering (Tianjin), Nankai University, Tianjin, China | [4]Institute of Molecular Engineering Plus, College of Chemistry, Fuzhou University, Fuzhou, China

Correspondence: Yu-Wu Zhong (zhongyuwu@fzu.edu.cn) | Kang Cai (kangcai@nankai.edu.cn) | Jie Shen (shenjie@fzu.edu.cn)

Received: 9 May 2026 | **Revised:** 14 July 2026 | **Accepted:** 17 July 2026

Keywords: artificial ion channels | high selectivity | lithium transport | molecular triangle | supramolecular chemistry

ABSTRACT

A central challenge in engineering artificial ion channels is the simultaneous achievement of high ion transport efficiency and high selectivity. In this study, we report a unimolecular Li^+ channel based on a rigid, C_3-symmetric pyromellitic diimide molecular triangle. The structure features a defined wall height of 2.2 nm and a narrow 4.1 Å pore lined with electron-rich carbonyl oxygens. Single-channel measurements reveal ultrafast Li^+ transport with a conductance of 57.4 pS—2.5 times that of gramicidin A-mediated K^+ conductance—alongside the record-high selectivity ratios of 50.1 for Li^+/Na^+ and 171.4 for Li^+/K^+. These performance metrics place this system among the most efficient and selective artificial Li^+ channels reported to date, while establishing a versatile molecular platform for Li^+-selective membranes and targeted therapeutics.

1 | Introduction

Ion channel proteins act as nature's exquisite gatekeepers, regulating ion flux across cell membranes with remarkable efficiency and selectivity. Their activity is dynamically modulated by diverse physiological stimuli—including voltage changes, ligand binding, and mechanical stress—making them essential to fundamental biological processes such as neural communication and muscle contraction [1–5]. Inspired by these sophisticated biological paradigms, the creation of artificial transmembrane ion transporters has evolved into an active frontier in supramolecular chemistry, leading to substantial progress [6–37].

Constructing a transmembrane channel from a single covalently linked molecule offers distinct advantages, including intrinsic structural integrity, a well-defined and deterministic architecture, and consequently more direct structure–property relationships [14, 24, 29–35]. Representative examples include pillar[*n*]arenes [38–40], aromatic foldamers [41–45], molecular cages [46, 47], hourglass-shaped systems [48], bottlebrush polymers [49], butterfly-shaped dendrimer [50], and polymers of intrinsic microporosity [51–54].

Significant progress has been achieved in the transmembrane transport of alkali metal ions. Advanced artificial K^+ channels now exhibit K^+/Na^+ selectivity ratios of up to 153.2 [53], representing a substantial improvement over earlier systems (9.8 [55], 16.3 [41], and 41.3 [50]). Similarly, artificial Na^+ channels have shown marked advances, with Na^+/K^+ selectivity increasing from 13 in 2024 [56] to 37.8 in 2026 [54]. In addition, the first artificial Cs^+

Mingju Luo and Si-Dan Guo contributed equally to this work.

channel has recently been reported, displaying selectivity ratios of 32.1 for Cs^+/Na^+ and 2.7 for Cs^+/K^+ [57].

Despite the absence of natural Li^+ channels [58] and the intrinsic challenges associated with Li^+ (high charge density and large dehydration energy), notable progress has also been made in artificial Li^+ channels [45, 51, 52, 59], with the highest Li^+/Na^+ and Li^+/K^+ selectivity ratios reaching approximately 43.8 and 51.6, respectively [47].

As a frontline treatment for bipolar disorder, Li^+ suffers from intrinsically poor membrane permeability, arising from the absence of dedicated natural channels [60]—which necessitates relatively high therapeutic concentrations (0.6–1.2 mM) and often leads to significant side effects [61]. Artificial Li^+ channels could provide a promising solution by enabling efficient transmembrane transport, thereby enhancing cellular uptake, reducing required dosages, and mitigating toxicity. Beyond biomedical relevance, the rapidly increasing demand for lithium in sustainable energy technologies further highlights the need for highly selective separation membranes, particularly for lithium extraction from brines and seawater, where Li^+ is vastly outnumbered by Na^+ and K^+ [62]. In this context, we aim to develop next-generation Li^+-transporting channels that combine high conductance with exceptional selectivity, a persistent challenge in this field.

As an intriguing class of cavity-containing aromatic scaffolds [63, 64], pyromellitic diimide (PMDI)-based triangular macrocycles merit investigation. Their rigid, π-electron-rich aromatic frameworks can span lipid membranes, making them promising candidates for transmembrane channel construction with precise structural control and well-defined cation-binding environments.

In this study, we present two novel C_3-symmetric triangular molecules **1** and **2** based on a PMDI core peripherally functionalized with phenyl rings (Figure 1a). These molecules adopt a unimolecular tubular architecture featuring a rigid, preorganized wall of 2.2 nm and a constricted pore of only 4.1 Å, structurally mimicking the narrow selectivity filter of biological aquaporin water channels [65] or potassium channels [66]. Lining the pore, the inwardly oriented carbonyl oxygen atoms create a polar and interactive interior that provides suitable binding sites for selective cation–dipole interactions. Single channel current measurements reveal that **1** enables ultrafast and highly selective Li^+ transport, with a conductance of 57.4 pS that is the second-highest value reported to date among artificial Li^+ channels [45, 47, 51, 52, 59] and 2.5 times that of gramicidin A-mediated K^+ conductance [55]. It also exhibits the record-high selectivity ratios of 50.1 for Li^+/Na^+ and 171.4 for Li^+/K^+. These functional properties establish a promising platform for future applications, ranging from therapeutic strategies that target Li^+ channels [60, 61] to the development of Li^+-selective membranes [62].

2 | Results and Discussion

2.1 | Molecular Design and Synthesis

The PMDI-based molecular triangle we designed combines exceptional structural stability with a pre-organized aromatic pore and the potential for vertical extension to better match the hydrophobic thickness of biological membranes. This architecture can be realized through a [3+3] cyclization of PMDI with (*R,R*)- or (*S,S*)-1,2-cyclohexanediamine, affording the chiral molecular triangles (*R,R*)- and (*S,S*)-**PMDI-Br**. In these structures, three PMDI units are bridged by acetylene spacers to peripheral phenyl rings, yielding two discrete configurations—**1** (*R,R*) and **2** (*S,S*)—each forming a stable tubular architecture (Figure 1a; Figures S1 and S3). The synthesis of **1** or **2** requires a synthetically demanding sixfold Sonogashira coupling of the brominated PMDI triangular precursor, during which partially substituted intermediates can form and contribute to the complex product distribution and relatively low isolated yields (Figure S2). Molecular electrostatic potential analysis [67] reveals a highly negative electrostatic potential localized on the carbonyl oxygen atoms of the PMDI framework (Figure 1b). This characteristic provides potent binding sites for ions, while the possibly distinct binding energy differences between various cations and the oxygen atoms form the basis for highly selective ion transport. The resulting channel exhibits a constricted pore diameter of ~4 Å and a total molecular height of 2.2 nm (Figure 1c), which is shorter than the hydrophobic core of approximately 3 nm thick for a DOPC bilayer [68, 69]. Nevertheless, efficient ion transport does not necessarily require a continuous channel lumen spanning the entire membrane thickness. As demonstrated by Voyer and co-workers, a Na^+ ion can traverse approximately 11 Å (1.1 nm) between two binding sites within the hydrophobic interior of a lipid bilayer through a hopping mechanism [70]. Accordingly, numerous artificial ion channel systems with continuous channel lumens spanning only 2–3 nm have been reported and nevertheless exhibit excellent ion transport activity [41, 43, 45, 71, 72].

Moreover, molecular dynamics (MD) simulations [73] show that the 2.2 nm-long molecule remains stably embedded in the bilayer throughout the 200 ns MD simulation, maintaining a well-defined orientation within the membrane (Figure S12). This persistent membrane positioning generates a structurally defined cavity located in the hydrophobic core of the bilayer, possibly facilitating selective ion binding and translocation across the membrane (Figure 1d).

Although the arylacetylene-modified molecular triangle exists in two chiral configurations as seen in **1** and **2**, their performance in transporting achiral alkali metal ions across membranes should, in principle, show no difference. However, given the overall *R*-chirality of DOPC lipids [74], it is reasonable to assume that **1** and **2** might exhibit differential functional behaviors in DOPC membranes, not only in their membrane incorporation efficiency but also in their membrane interactions and intra-membrane orientation/distribution.

To test this hypothesis, we first measured the fluorescence intensities of **1** and **2** in buffer solution (100 mM LiCl, 10 mM HEPES, pH = 8.0) and after premixing with DOPC lipids (Figure S10). The results show that although **1** and **2** exhibit nearly identical fluorescence intensities under the same condition—whether measured in buffer solution or after premixing with DOPC—the premixing procedure leads to significant fluorescence quenching compared to their fluorescence in buffer solution. To further probe the distinct membrane behaviors of

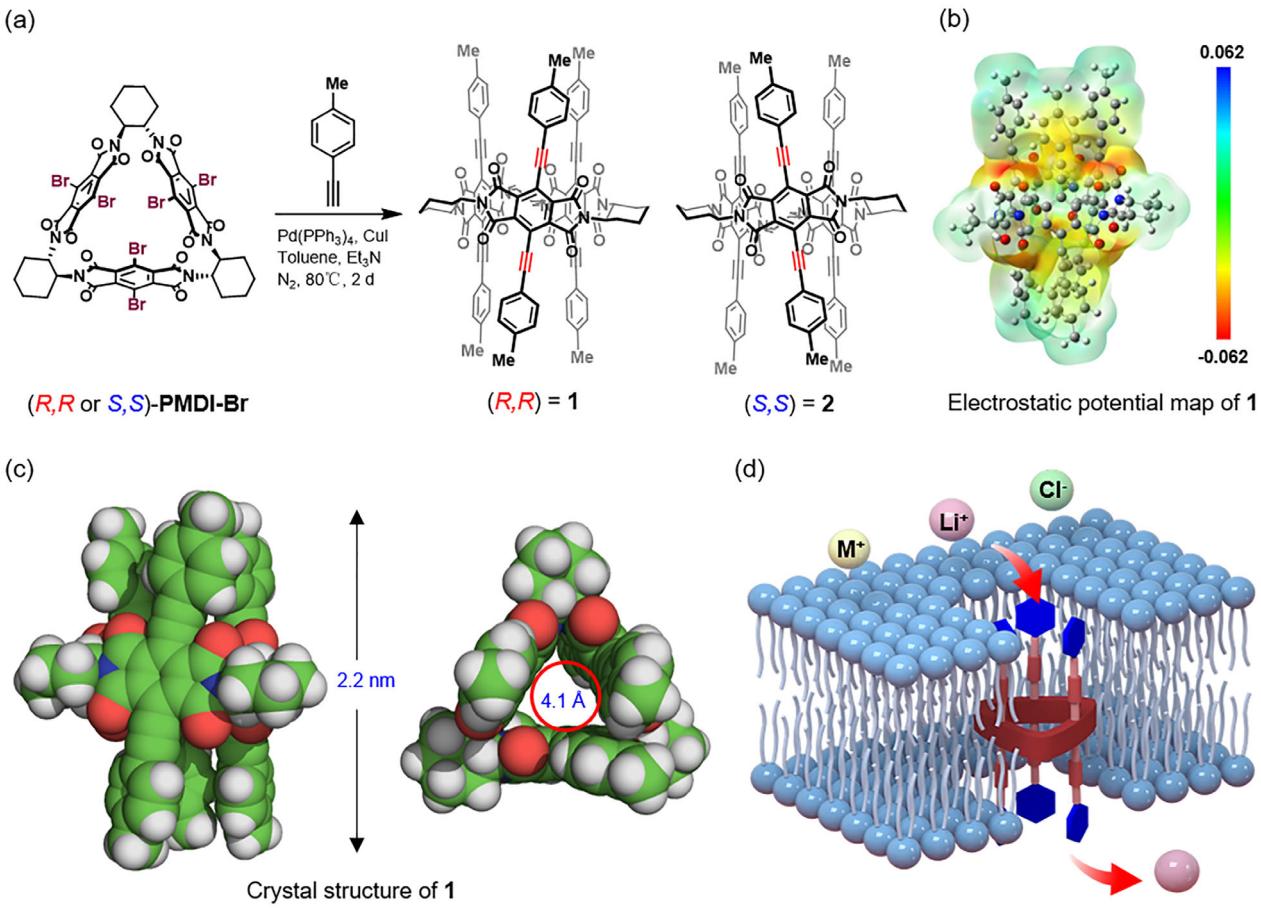

FIGURE 1 | (a) Molecular design and synthetic construction of molecular triangles **1** and **2**. (b) Electrostatic potential map of **1** shows the electron-rich nature of the central cavity, suggesting its affinity for cations. (c) Crystal structure of **1** (CCDC no. 2549844), illustrating a height of 2.2 nm and an internal cavity diameter of 4.1 Å. (d) Schematic illustration of 1-mediated transmembrane Li^+ transport.

1 and **2**, their THF solutions were added to suspensions of DOPC-containing LUVs, and the fluorescence changes were monitored immediately. At concentrations above 0.5 μM, **1** exhibits significantly lower fluorescence intensity than **2**, suggesting differential membrane insertion and/or chirality-dependent organization-induced quenching (Figure S10b). This interpretation is further supported by CD titration experiments (Figure S11): upon binding to DOPC liposomes, **1** shows a progressive increase in CD signal, whereas **2** exhibits a progressive decrease (Figure S11c), indicating distinct chiral supramolecular arrangements within the membrane. The binding free energies were determined to be −7.68 kcal/mol for **1** and −7.26 kcal/mol for **2** (Figure S11d,e), with DOPC exhibiting an approximately twofold stronger chiral preference for the *R*-enantiomer **1** than for the *S*-enantiomer **2**. These observations demonstrate that the functional difference between the two enantiomers arises not merely from differences in insertion efficiency, but also from fundamentally different membrane association and supramolecular organization.

2.2 | Ion Transport Activity of Molecular Triangles 1 and 2

The ion transport activity and selectivity of **1** and **2** were investigated using a fluorescence-based vesicle assay. The DOPC vesicles encapsulate the pH-sensitive HPTS dye, establishing a transmembrane proton gradient of 7.0 to 8.0 in pH. With an external buffer containing 100 mM MCl (M = Li, Na, K, Rb, and Cs), **1** and **2** display preferential transport of Li^+ (Figures 2a and S4b). Notably, **1** demonstrates remarkably high Li^+ transport efficiency, reaching 80% (Figure 2a) after subtracting background signals (Figure S4a), which is in sharp contrast to the considerably lower values observed for other cations: Na^+ (19%), K^+ (23%), Rb^+ (14%), and Cs^+ (34%). Under identical conditions, **2** also transports Li^+ preferentially, though with significantly lower activity (38%), alongside efficiencies of 28% for Na^+, 17% for K^+, 19% for Rb^+, and 30% for Cs^+ (Figures 2a and S4b). These marked differences in activity arise from distinct membrane interactions—association, orientation, and partitioning—that collectively govern the transport behavior of **1** and **2**. Furthermore, Hill analysis of the Li^+ transport activity mediated by **1** affords an EC_{50} value of 0.43 μM, corresponding to a channel-to-lipid molar ratio of 0.6% (e.g., 0.43/(96 × 0.77)) after correction for the 23% loss of DOPC lipids during the extrusion process (Figures S4c and S11a,b).

The anion transport properties of **1** and **2** were verified using the Cl–sensitive SPQ assay, because the fluorescence intensity of SPQ decreases with increasing concentrations of Cl^- anions. The minimal changes in SPQ fluorescence intensity induced by both **1** and **2** are comparable to the background, confirming their inability to transport Cl^- (Figure 2b).

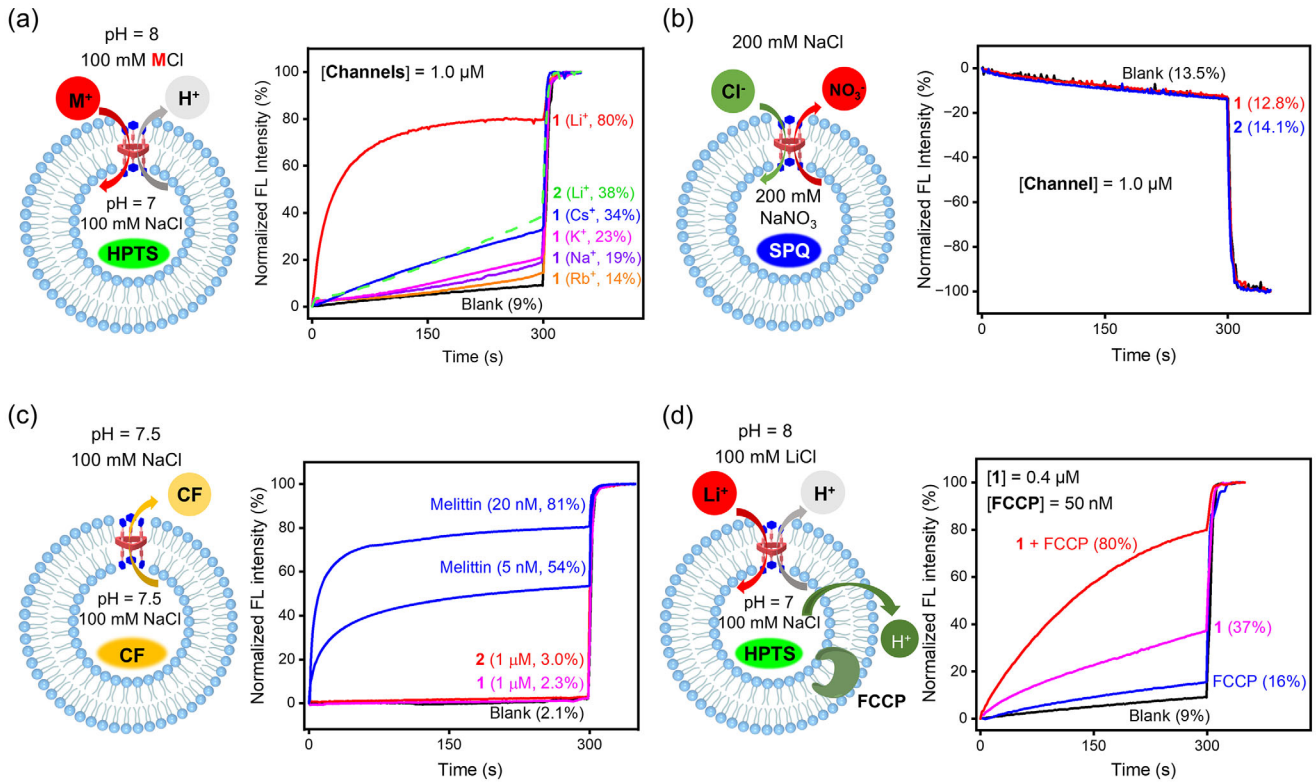

FIGURE 2 | (a) The pH-sensitive HPTS assay for assessing Li^+ transport selectivity of **1** in DOPC-based LUVs, with the extravesicular region varied to have 100 mM MCl (M = Li, Na, K, Rb, and Cs). (b) The chloride-sensitive SPQ assay to confirm negligible chloride transport activity by **1** and **2**. (c) The CF dye leakage assay to confirm the membrane integrity in the presence of **1** and **2**. (d) The HPTS assay using a proton carrier FCCP to compare the transport rate between H^+ and Li^+ mediated by **1** at 0.3 μM. DOPC = dioleoyl phosphatidylcholine; HPTS = 8-hydroxypyrene-1,3,6-trisulfonic acid trisodium salt; SPQ = 6-methoxy-*N*-(3-sulfopropyl) quinolinium; CF = 5(6)-carboxyfluorescein; FCCP = carbonyl cyanide 4-(trifluoromethoxy) phenylhydrazone.

To further exclude nonspecific membrane disruption by **1** and **2**, a CF leakage assay was performed using 5(6)-carboxyfluorescein (CF), a membrane-impermeable fluorescent dye (Figure 2c). The dye, which exists as two isomers (~9.2 × 11.4 Å and ~10 × 10 Å; Figure S5), was encapsulated within the intravesicular region at 50 mM, at which it undergoes self-quenching through dimerization. Because the external solution contains no CF, an outward transmembrane concentration gradient of CF is established. If membrane disruption occurs, CF leaks out of the vesicles, resulting in dilution of the dye, dissociation of self-quenched dimers into highly fluorescent monomers, and a corresponding increase in fluorescence intensity. This assay therefore provides a sensitive measure of membrane integrity. As shown in Figures 2c and S5, both **1** and **2** at 1 μM induce statistically insignificant changes in CF fluorescence intensity. In contrast, the pore-forming peptide melittin, employed as a positive control, causes significant fluorescence increases of 54% and 81% at concentrations of 5 and 20 nM, respectively. These results conclusively establish that **1** and **2** preserve the integrity of LUVs membranes and mediate ion transport through specific transporter-mediated activity rather than via nonspecific membrane disruption.

To compare the relative transport rate between Li^+ and H^+, HPTS assays were conducted in the presence of a protonophore FCCP (Figure 2d). FCCP accelerates proton delayed H^+ counter-transport during Li^+ influx, producing fluorescence enhancement. The transport efficiencies are 7.7% ((16%–9%)/0.91) for FCCP alone, and 31% for **1** alone. In the presence of FCCP, **1** exhibits markedly enhanced efficiency of 40% ((80%–37%—(16%–9%))/0.91). This significant enhancement confirms that Li^+ flux is the dominant process.

Although pre-incorporation of **1** or **2** with DOPC lipids yields nearly identical initial channel-to-lipid ratios and comparable fluorescence intensities (Figure S6a), this protocol did not provide a reliable basis for quantitative transport comparison. Non-extruded vesicles show heterogeneous morphology and poorly reproducible HPTS responses across independent measurements (Figure S6b,c), whereas pre-incorporation followed by extrusion caused loss of channel-containing lipid material, as evidenced by yellowish residue retained on the polycarbonate membrane (Figure S6d). Thus, the final functional channel-to-lipid ratios after extrusion cannot be assumed to remain identical to the initial premixed ratios. Importantly, even under these conditions, **1** still shows higher ion transport activity than **2** (Figure S6e,f), consistent with the activity trend observed in Figure 2a.

2.3 | Molecular Triangle 1 Functions as a Highly Selective Li^+ Channel

As revealed by the crystal structure (Figure 1c), **1** encloses a membrane-spanning hollow cavity rich in cation-binding sites, leading to selective Li^+ transport as shown by the HPTS assay (Figure 2a). To quantify the transport selectivity ratios, we

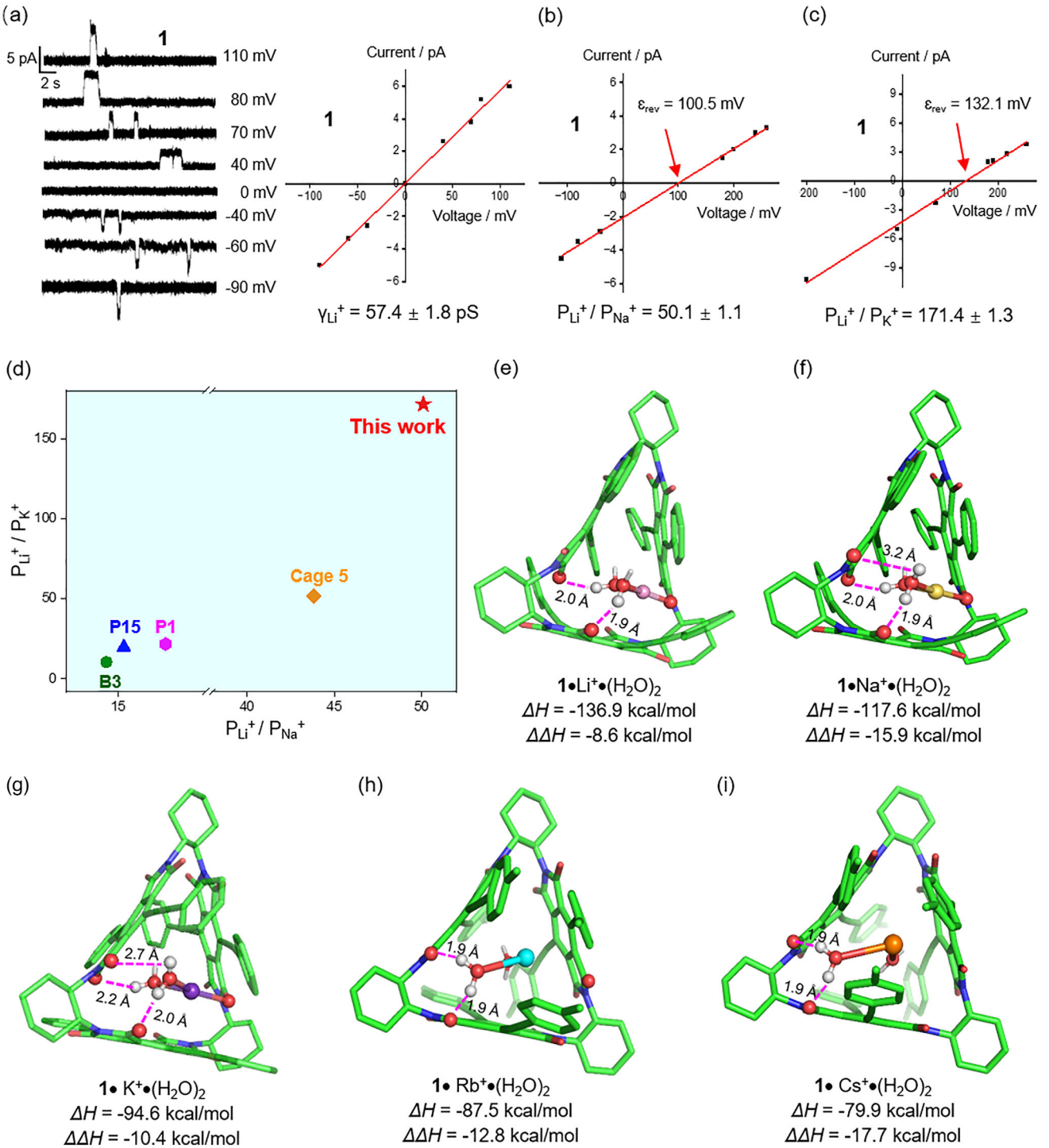

FIGURE 3 | (a) Single channel current traces and I–V curve (cis chamber = trans chamber = 1.0 M LiCl) from which the γLi^+ value for **1** was determined to be 57.4 ± 1.8 pS. (b) *I–V* curve (cis chamber = 1.0 M NaCl, trans chamber = 1.0 M LiCl) from which Li^+/Na^+ (PLi^+/PNa^+) selectivity value for **1** was determined to be 50.1 ± 1.1. (c) *I–V* curve (cis chamber = 1.0 M KCl, trans chamber = 1.0 M LiCl) from which Li^+/K^+ (PLi^+/PK^+) selectivity value for **1** was determined to be 171.4 ± 1.3. Here, γLi^+ values were obtained by fitting the *I–V* curve using a linear equation of $y = a + b*x$ where slope b is γLi^+ in the unit of pS. In (b) and (c), the permeability ratio (PLi^+/PM^+) was calculated using a simplified Goldman–Hodgkin–Katz equation $\varepsilon rev = RT/F \times \ln(PLi^+/PM^+)$, where R = universal gas constant (8.314 J K^{-1} mol^{-1}), T = 298 K, F = Faraday's constant (96485 C mol^{-1}), and P is the permeability of the ions. (d) Li^+/Na^+ and Li^+/K^+ selectivity values for reported artificial Li^+ channels (B3,51 P15,45 P1,52 and Cage 547) versus this work. (e–i) Coordination models of Li^+, Na^+, K^+, Rb^+, and Cs^+ with 1. Color code: Li, pink; Na, yellow; K, purple; Rb, cyan; Cs, orange; N, blue; C, green; O, red; H, white. Most H-atoms have been removed for clarity of view.

performed single-channel recordings on planar lipid bilayers composed of DOPC. Under symmetric salt conditions (1 M LiCl in both cis and trans chambers, Figure S7), **1** exhibits well-defined, rectangular current transitions characteristic of single-channel behavior at voltages ranging from +100 mV to −100 mV. Analysis of the current–voltage (*I–V*) relationship yields a unitary Li^+ conductance ($\gamma_{Li}{}^+$) of 57.4 ± 1.8 pS (Figure 3a)—2.5 times that of gramicidin A-mediated K^+ conductance [55] and the second-highest value, following 104.4 pS reported by our group [52]. This conductance corresponds to a flux of 3.6×10^7 Li^+ s^{-1} at 100 mV.

The Li^+/Na^+ and Li^+/K^+ selectivity ratios ($P_{Li}{}^+/P_{Na}{}^+$) and ($P_{Li}{}^+/P_K{}^+$) were determined under bi-ionic conditions, where the trans chamber contained 1.0 M LiCl and the cis chamber contained either 1.0 M NaCl or 1.0 M KCl (Figures S8 and S9). From the resulting *I–V* curves (Figure 3b,c), the reversal potentials (ε_{rev}) were determined to be +100.5 mV (vs. NaCl gradient) and +132.1 mV (vs. KCl gradient). Application of the Goldman-Hodgkin-Katz equation yields Li^+/Na^+ and Li^+/K^+ selectivity ratios of 50.1 ± 1.1 and 171.4 ± 1.3, respectively. These values confirm the highest Li^+/Na^+ selectivity and Li^+/K^+ selectivity reported to date for artificial Li^+ channels, surpassing the previously reported ranges of 14.3–43.8 for Li^+/Na^+ and 10.5–51.6 for Li^+/K^+, respectively (Figure 3d) [45, 47, 51, 52, 59].

This performance highlights its ability to combine high conductance with exceptional selectivity, bringing artificial ion channels one step closer to overcoming the persistent challenge of simultaneously achieving high ionic flux and high selectivity.

2.4 | Mechanistic Insights into Selective Li^+ Transport by Molecular Triangle 1

DFT calculations were performed to elucidate the ion-binding interactions involved in the selective Li^+ transport mediated by molecular triangle **1**. The reliability of the enthalpy calculations was first evaluated by comparing the computed hydration enthalpies of $M^+\bullet(H_2O)_6$ complexes with reported experimental values for M = Li, Na, K, Rb, and Cs, which showed good agreement (Table S2). Among the $\mathbf{1}\bullet M^+\bullet(H_2O)_n$ (n = 0–3) complexes, the trihydrated complexes are not sterically compatible with the narrow triangular cavity of **1** (Figure S14).

With the enthalpy change of $\Delta\Delta H$ defined as the enthalpy difference between the partially hydrated $\mathbf{1}\bullet M^+\bullet(H_2O)_n$ complex and the corresponding fully hydrated $M^+\bullet(H_2O)_6$ complex, the calculated $\Delta\Delta H$ values for the fully dehydrated $\mathbf{1}\bullet M^+$ complexes are positive for all ions (Table S3), indicating that complete dehydration is energetically unfavorable. The monohydrated $\mathbf{1}\bullet M^+\bullet(H_2O)$ complexes also give positive $\Delta\Delta H$ values for Li^+, Na^+, K^+, and Rb^+, except for Cs^+ giving a slightly negative value of −4.1 kcal/mol. In contrast, the dihydrated $\mathbf{1}\bullet M^+\bullet(H_2O)_2$ complexes give negative $\Delta\Delta H$ values for all five alkali-metal ions, with the energetic gains of −8.6, −15.9, −10.4, −12.8, and −17.7 kcal/mol for Li^+, Na^+, K^+, and Rb^+, and Cs^+, respectively (Figure 3e–i and Table S3). These results suggest that the dihydrated state provides a reasonable common model that balances steric compatibility within the confined pore with energetic compensation for partial dehydration. Nevertheless, it should be noted that, these gas-phase optimized structures are meant to offer useful structural insights into ion coordination and translocation through the channel, they cannot be directly used to compare the transport preferences of different ions.

To better recapitulate the ion-transporting membrane environment, we have determined the binding constants of **1** toward alkali metal ions in DOPC LUVs (Figure S15–S17). The obtained binding constants increase in the order: Cs^+ (4.0×10^3 M^{-1}) < Rb^+ (4.4×10^3 M^{-1}) < K^+ (5.7×10^3 M^{-1}) < Na^+ (6.4×10^3 M^{-1}) < Li^+ (1.6×10^4 M^{-1}).

Notably, neither the $\Delta\Delta H$ values ($Cs^+ > Na^+ > Rb^+ > K^+ > Li^+$) nor the binding constants ($Li^+ > Na^+ > K^+ > Rb^+ > Cs^+$) alone show a simple correlation with the experimentally observed transport efficiencies ($Li^+ > Cs^+ > K^+ > Na^+ > Rb^+$). Therefore, the observed transport efficiency order should be understood as the result of multiple factors, including partial dehydration, membrane-based ion affinity, steric compatibility within the pore, and ion-release dynamics. Li^+ benefits from the highest membrane-based affinity toward **1**, which favors selective capture and helps offset its high dehydration cost. In addition, its small ionic radius and high charge density may allow Li^+ to adopt a compact coordination environment within the confined PMDI-lined pore, while local coordination flexibility and hydration-water exchange may contribute to translocation after partial dehydration [75–78]. In contrast, weakly bound Cs^+ has a lower dehydration penalty and may be released more readily after entering the channel, accounting for its relatively high transport efficiency. By comparison, Na^+, K^+, and Rb^+ do not appear to achieve the same balance among dehydration, binding, and release, appear to lower overall transport efficiencies.

3 | Summary

In this study, we report the rational design of rigid, C_3-symmetric molecular triangles (**1** and **2**) constructed from pyromellitic diimide units. This unimolecular channel features a precisely defined membrane-spanning scaffold of 2.2 nm and a constricted 4.1 Å pore lined with electron-rich oxygen atoms. Single-channel measurements show that **1** mediates ultrafast Li^+ transport with a conductance of 57.4 pS and exhibits the highest selectivity ratios of 50.1 for Li^+ over Na^+ and 171.4 for Li^+ over K^+, placing it among the most efficient artificial Li^+ channels reported to date. These results highlight the critical role of preorganized aromatic microcavities in enabling highly selective and efficient ion transport, and establish a new design paradigm for applications in biomedicine and ion-selective separation membranes.

Author Contributions

Mingju Luo: data curation, formal analysis. **Si-Dan Guo:** methodology, validation. **Junhao Zhang:** data curation. **Wenju Chang:** validation. **Dong-Sheng Guo:** conceptualization. **Yu-Wu Zhong:** formal analysis, writing – review and editing. **Kang Cai:** conceptualization, writing – review and editing. **Jie Shen:** writing – original draft, writing – review and editing, supervision. **Huaqiang Zeng:** writing – review and editing, supervision.

Acknowledgments

We greatly appreciate the support of this work by the National Natural Science Foundation of China (22271049 and 22371048), the Natural Science Foundation of Fujian Province (2023J01054), the "Chu Ying Program" for the Top Young Talents of Fujian Province, and a start-up grant from Fuzhou University.

Conflicts of Interest

The authors declare no conflicts of interest.

Data Availability Statement

The data that support the findings of this study are available from the corresponding author upon reasonable request.

References

1. M. Piccolino, "Biological Machines: From Mills to Molecules," *Nature Reviews Molecular Cell Biology* 1 (2000): 149–152, https://doi.org/10.1038/35040097.

2. J. J. Kasianowicz, "Introduction to Ion Channels and Disease," *Chemical Reviews* 112 (2012): 6215–6217, https://doi.org/10.1021/cr300444k.

3. K. A. Muraglia, R. S. Chorghade, B. R. Kim, et al., "Small-Molecule Ion Channels Increase Host Defences in Cystic Fibrosis Airway Epithelia," *Nature* 567 (2019): 405–408, https://doi.org/10.1038/s41586-019-1018-5.

4. S. M. Emrich, R. E. Yoast, and M. Trebak, "Physiological Functions of CRAC Channels," *Annual Review of Physiology* 84 (2022): 355–379, https://doi.org/10.1146/annurev-physiol-052521-013426.

5. J. Huang, X. Pan, and N. Yan, "Structural Biology and Molecular Pharmacology of Voltage-Gated Ion Channels," *Nature Reviews Molecular Cell Biology* 25 (2024): 904–925, https://doi.org/10.1038/s41580-024-00763-7.

6. A. P. Davis, D. N. Sheppard, and B. D. Smith, "Development of Synthetic Membrane Transporters for Anions," *Chemical Society Reviews* 36 (2007): 348–357, https://doi.org/10.1039/B512651G.

7. S. Matile, A. Vargas Jentzsch, J. Montenegro, and A. Fin, "Recent Synthetic Transport Systems," *Chemical Society Reviews* 40 (2011): 2453–2453, https://doi.org/10.1039/c0cs00209g.

8. B. Chunyan, J. Huijuan, L. Tao, W. Yi, P. Wei, and Z. Linyong, "Synthesis of Artificial Ion Channels in Bilayer Membrane," *Progress in Chemistry* 24 (2012): 1337–1345.

9. F. Otis, M. Auger, and N. Voyer, "Exploiting Peptide Nanostructures To Construct Functional Artificial Ion Channels," *Accounts of Chemical Research* 46 (2013): 2934–2943, https://doi.org/10.1021/ar400044k.

10. J. Montenegro, M. R. Ghadiri, and J. R. Granja, "Ion Channel Models Based on Self-Assembling Cyclic Peptide Nanotubes," *Accounts of Chemical Research* 46 (2013): 2955–2965, https://doi.org/10.1021/ar400061d.

11. T. M. Fyles, "How Do Amphiphiles Form Ion-Conducting Channels in Membranes? Lessons From Linear Oligoesters," *Accounts of Chemical Research* 46 (2013): 2847–2855, https://doi.org/10.1021/ar4000295.

12. N. Sakai and S. Matile, "Synthetic Ion Channels," *Langmuir* 29 (2013): 9031–9040, https://doi.org/10.1021/la400716c.

13. B. Gong and Z. Shao, "Self-Assembling Organic Nanotubes With Precisely Defined, Sub-Nanometer Pores: Formation and Mass Transport Characteristics," *Accounts of Chemical Research* 46 (2013): 2856–2866, https://doi.org/10.1021/ar400030e.

14. W. Si, P. Xin, Z.-T. Li, and J.-L. Hou, "Tubular Unimolecular Transmembrane Channels: Construction Strategy and Transport Activities," *Accounts of Chemical Research* 48 (2015): 1612–1619, https://doi.org/10.1021/acs.accounts.5b00143.

15. B. Gong, "Artificial Water Channels: Inspiration, Progress, and Challenges," *Faraday Discussions* 209 (2018): 415–427, https://doi.org/10.1039/C8FD00132D.

16. H. Gill, M. R. Gokel, M. McKeever, et al., "Supramolecular Pore Formation as an Antimicrobial Strategy," *Coordination Chemistry Reviews* 412 (2020): 213264, https://doi.org/10.1016/j.ccr.2020.213264.

17. J. T. Davis, P. A. Gale, and R. Quesada, "Advances in Anion Transport and Supramolecular Medicinal Chemistry," *Chemical Society Reviews* 49 (2020): 6056–6086, https://doi.org/10.1039/C9CS00662A.

18. S.-P. Zheng, L.-B. Huang, Z. Sun, and M. Barboiu, "Self-Assembled Artificial Ion-Channels Toward Natural Selection of Functions," *Angewandte Chemie International Edition* 60 (2021): 566–597, https://doi.org/10.1002/anie.201915287.

19. J. Yang, G. Yu, J. L. Sessler, I. Shin, P. A. Gale, and F. Huang, "Artificial Transmembrane Ion Transporters as Potential Therapeutics," *Chemistry* 7 (2021): 3256–3291, https://doi.org/10.1016/j.chempr.2021.10.028.

20. A. Roy and P. Talukdar, "Recent Advances in Bioactive Artificial Ionophores," *ChemBioChem* 22 (2021): 2925–2940, https://doi.org/10.1002/cbic.202100112.

21. W. Song and M. Kumar, "Beyond Aquaporins: Recent Developments in Artificial Water Channels," *Langmuir* 38 (2022): 9085–9091, https://doi.org/10.1021/acs.langmuir.2c01605.

22. J. Shen, C. Ren, and H. Zeng, "Membrane-Active Molecular Machines," *Accounts of Chemical Research* 55 (2022): 1148–1159, https://doi.org/10.1021/acs.accounts.1c00804.

23. A. Mondal, M. Ahmad, D. Mondal, and P. Talukdar, "Progress and Prospects Toward Supramolecular Bioactive Ion Transporters," *Chemical Communications* 59 (2023): 1917–1938, https://doi.org/10.1039/D2CC06761G.

24. L. He, T. Zhang, C. Zhu, T. Yan, and J. Liu, "Crown Ether-Based Ion Transporters in Bilayer Membranes," *Chemistry—A European Journal* 29 (2023): e202300044, https://doi.org/10.1002/chem.202300044.

25. M. Ahmad, S. A. Gartland, and M. J. Langton, "Photo- and Redox-Regulated Transmembrane Ion Transporters," *Angewandte Chemie International Edition* 62 (2023): e202308842, https://doi.org/10.1002/anie.202308842.

26. J. de Jong, J. E. Bos, and S. J. Wezenberg, "Stimulus-Controlled Anion Binding and Transport by Synthetic Receptors," *Chemical Reviews* 123 (2023): 8530–8574, https://doi.org/10.1021/acs.chemrev.3c00039.

27. K. Norvaisa, A. Torres-Huerta, and H. Valkenier, "Synthetic Transporters for Oxoanions," *Current Opinion in Chemical Biology* 83 (2024): 102542, https://doi.org/10.1016/j.cbpa.2024.102542.

28. S. Ren, Z. Zhang, and Z. Dong, "Biomimetic Ion Channels: An Emerging and Promising Material for Therapeutic Ion Channelopathies," *Trends in Chemistry* 6 (2024): 726–738, https://doi.org/10.1016/j.trechm.2024.10.005.

29. X. Yuan, J. Shen, and H. Zeng, "Artificial Transmembrane Potassium Transporters: Designs, Functions, Mechanisms and Applications," *Chemical Communications* 60 (2024): 482–500, https://doi.org/10.1039/D3CC04488B.

30. D. Zhang, W. Chang, J. Shen, and H. Zeng, "Aromatic Foldamer-Derived Transmembrane Transporters," *Chemical Communications* 60 (2024): 13468–13491, https://doi.org/10.1039/D4CC04388J.

31. K. Sato, "Beyond Natural Channel Proteins: Recent Advances in Fluorinated Nanochannels," *Langmuir* 40 (2024): 2809–2814, https://doi.org/10.1021/acs.langmuir.3c03665.

32. D.-D. Su and M. Barboiu, "Hydrogen-Bonded Water-Wires/Clusters—Toward Natural Selectivity of Artificial Water Channels," *Coordination Chemistry Reviews* 515 (2024): 215973, https://doi.org/10.1016/j.ccr.2024.215973.

33. I. Zubair, L. Martínez-Crespo, and S. J. Webb, "Foldamer-Mediated Transport Across Phospholipid Bilayers," *Current Opinion in Chemical Biology* 84 (2025): 102549, https://doi.org/10.1016/j.cbpa.2024.102549.

34. A. Kohata and K. Kinbara, "Synthetic Ion Channels in Biomembranes," *Current Opinion in Chemical Biology* 84 (2025): 102544, https://doi.org/10.1016/j.cbpa.2024.102544.

35. T. Yan and J. Liu, "Transmembrane Ion Channels: From Natural to Artificial Systems," *Angewandte Chemie International Edition* 64 (2025): e202416200, https://doi.org/10.1002/anie.202416200.

36. W. Huang, C. Jia, and C. Ren, "Artificial Ion Transporters as Potent Therapeutics for Channelopathies," *ChemMedChem* 20 (2025): e202400811, https://doi.org/10.1002/cmdc.202400811.

37. U. M. C. Rathnaweera, S. M. Chowdhury, R. Salam, and N. Busschaert, "Medical and Nonmedical Applications of Synthetic Transmembrane Anion Transporters," *Chemical Reviews* 125 (2025): 8370–8425, https://doi.org/10.1021/acs.chemrev.5c00129.

38. W.-X. Feng, Z. Sun, Y. Zhang, et al., "Bis-15-Crown-5-Ether-Pillar[5]Arene K^+-Responsive Channels," *Organic Letters* 19 (2017): 1438–1441, https://doi.org/10.1021/acs.orglett.7b00352.

39. W. Song, H. Joshi, R. Chowdhury, et al., "Artificial Water Channels Enable Fast and Selective Water Permeation Through Water-Wire Networks," *Nature Nanotechnology* 15 (2020): 73–79, https://doi.org/10.1038/s41565-019-0586-8.

40. L. Shi, W. Zhao, Z. Jiu, et al., "Redox-Regulated Synthetic Channels: Enabling Reversible Ion Transport by Modulating the Ion-Permeation Pathway," *Angewandte Chemie International Edition* 63 (2024): e202403667, https://doi.org/10.1002/anie.202403667.

41. F. Chen, J. Shen, N. Li, et al., "Pyridine/Oxadiazole-Based Helical Foldamer Ion Channels With Exceptionally High K^+/Na^+ Selectivity," *Angewandte Chemie International Edition* 59 (2020): 1440–1444, https://doi.org/10.1002/anie.201906341.

42. A. Roy, J. Shen, H. Joshi, et al., "Foldamer-Based Ultrapermeable and Highly Selective Artificial Water Channels that Exclude Protons," *Nature Nanotechnology* 16 (2021): 911–917, https://doi.org/10.1038/s41565-021-00915-2.

43. T. Yan, S. Liu, J. Xu, H. Sun, S. Yu, and J. Liu, "Unimolecular Helix-Based Transmembrane Nanochannel With a Smallest Luminal Cavity of 1 Å Expressing High Proton Selectivity and Transport Activity," *Nano Letters* 21 (2021): 10462–10468, https://doi.org/10.1021/acs.nanolett.1c03858.

44. J. Shen, R. Ye, Z. Liu, and H. Zeng, "Hybrid Pyridine–Pyridone Foldamer Channels as M2-Like Artificial Proton Channels," *Angewandte Chemie International Edition* 61 (2022): e202200259, https://doi.org/10.1002/anie.202200259.

45. J. Shen, D. R, Z. Li, et al., "Sulfur-Containing Foldamer-Based Artificial Lithium Channels," *Angewandte Chemie International Edition* 62 (2023): e202305623, https://doi.org/10.1002/anie.202305623.

46. Y. D. Yuan, J. Dong, J. Liu, et al., "Porous Organic Cages as Synthetic Water Channels," *Nature Communications* 11 (2020): 4927, https://doi.org/10.1038/s41467-020-18639-7.

47. Y. Xu, Z. Luo, Q. Liu, et al., "High-Performance Artificial Lithium Channel Enabled by a Brominated Organic Imine Cage," *Angewandte Chemie International Edition* 65 (2026): e2715806, https://doi.org/10.1002/anie.2715806.

48. J.-F. Lin, X.-D. Wang, Y.-F. Ao, Q.-Q. Wang, and D.-X. Wang, "Spontaneous Transition Between Multiple Conductance States and Rectifying Behaviors in an Artificial Single-Molecule Funnel," *Angewandte Chemie International Edition* 63 (2024): e202411702, https://doi.org/10.1002/anie.202411702.

49. Y. Lin, B. Wu, Y. Zeng, et al., "Artificial Channels Based on Bottlebrush Polymers: Enhanced Ion Transport Through Polymer Topology Control," *Angewandte Chemie International Edition* 63 (2024): e202408558, https://doi.org/10.1002/anie.202408558.

50. Y. Wu, Q. Xu, Y. Chen, et al., "Mechanosensitive and pH-Gated Butterfly-Shaped Artificial Ion Channel for High-Selective K^+ Transport and Cancer Cell Apoptosis," *Advanced Materials* 37 (2025): 2416852, https://doi.org/10.1002/adma.202416852.

51. F. Gou, Q. Wang, Z. Yang, W. Chang, J. Shen, and H. Zeng, "Artificial Lithium Channels Built From Polymers With Intrinsic Microporosity," *Angewandte Chemie International Edition* 64 (2025): e202418304, https://doi.org/10.1002/anie.202418304.

52. F. Gou, Z. Yang, Q. Wang, W. Chang, J. Shen, and H. Zeng, "Chirality-Induced Split Personality in Polymer With Intrinsic Microporosity-Based Artificial Ion Channels," *Angewandte Chemie International Edition* 64 (2025): e202516573, https://doi.org/10.1002/anie.202516573.

53. F. Gou, Y. Yao, Q. Wang, et al., "Flexible Crown-Ether Polyimides Break the K^+/Na^+ Selectivity Barrier in Artificial K^+ Channels," *Angewandte Chemie International Edition* 65 (2025): e20146, https://doi.org/10.1002/anie.202520146.

54. F. Gou, Y. Yao, Q. Wang, W. Chang, J. Shen, and H. Zeng, "Conformation-Adaptive Crown Ether-Polyimides as Superfast and Exceptionally Selective Artificial Na^+ Channels," *Angewandte Chemie International Edition* 65 (2026): e6835315, https://doi.org/10.1002/anie.6835315.

55. C. Ren, J. Shen, and H. Zeng, "Combinatorial Evolution of Fast-Conducting Highly Selective K^+ -Channels via Modularly Tunable Directional Assembly of Crown Ethers," *Journal of the American Chemical Society* 139 (2017): 12338–12341, https://doi.org/10.1021/jacs.7b04335.

56. L. Zhang, J. Tian, Z. Lin, and Z. Dong, "Efficient Sodium Transmembrane Permeation Through Helically Folded Nanopores With Natural Channel-Like Ion Selectivity," *Journal of the American Chemical Society* 146 (2024): 8500–8507, https://doi.org/10.1021/jacs.3c14736.

57. Z. Li, L. Yuan, P.-F. Li, et al., "Unanticipated Emergence of the Photo-Switchable Cs^+-Selective Ion Channels From One-Dimensional 18-Crown-6 Arrays," *Angewandte Chemie International Edition* 138 (2026): e5534613, https://doi.org/10.1002/anie.5534613.

58. I. Bukhteeva, F. A. Rahman, B. Kendall, et al., "Effects of Lithium Isotopes on Sodium/Lithium Co-Transport and Calcium Efflux Through the Sodium/Calcium/Lithium Exchanger in Mitochondria," *Frontiers in Physiology* 15 (2024): 1354091, https://doi.org/10.3389/fphys.2024.1354091.

59. L. Zhang, C. Zhang, X. Dong, and Z. Dong, "Highly Selective Transmembrane Transport of Exogenous Lithium Ions Through Rationally Designed Supramolecular Channels," *Angewandte Chemie International Edition* 62 (2023): e202214194, https://doi.org/10.1002/anie.202214194.

60. A. J. Ferrari, A. J. Baxter, and H. A. Whiteford, "A Systematic Review of the Global Distribution and Availability of Prevalence Data for Bipolar Disorder," *Journal of Affective Disorders* 134 (2011): 1–13, https://doi.org/10.1016/j.jad.2010.11.007.

61. M. Gitlin, "Lithium Side Effects and Toxicity: Prevalence and Management Strategies," *International Journal of Bipolar Disorders* 4 (2016): 27, https://doi.org/10.1186/s40345-016-0068-y.

62. C. Liu, Y. Li, D. Lin, et al., "Lithium Extraction From Seawater Through Pulsed Electrochemical Intercalation," *Joule* 4 (2020): 1459–1469, https://doi.org/10.1016/j.joule.2020.05.017.

63. D. J. Kim, K. R. Hermann, A. Prokofjevs, et al., "Redox-Active Macrocycles for Organic Rechargeable Batteries," *Journal of the American Chemical Society* 139 (2017): 6635–6643, https://doi.org/10.1021/jacs.7b01209.

64. Y. Wang, H. Wu, and J. F. Stoddart, "Molecular Triangles: A New Class of Macrocycles," *Accounts of Chemical Research* 54 (2021): 2027–2039, https://doi.org/10.1021/acs.accounts.1c00108.

65. D. Kozono, M. Yasui, L. S. King, and P. Agre, "Aquaporin Water Channels: Atomic Structure Molecular Dynamics Meet Clinical Medicine," *Journal of Clinical Investigation* 109 (2002): 1395–1399, https://doi.org/10.1172/JCI0215851.

66. D. Naranjo, H. Moldenhauer, M. Pincuntureo, and I. Díaz-Franulic, "Pore size Matters for Potassium Channel Conductance," *Journal of General Physiology* 148 (2016): 277–291, https://doi.org/10.1085/jgp.201611625.

67. P. Politzer, P. R. Laurence, and K. Jayasuriya, "Molecular Electrostatic Potentials: An Effective Tool for the Elucidation of Biochemical Phenomena," *Environmental Health Perspectives* 61 (1985): 191–202, https://doi.org/10.1289/ehp.8561191.

68. J. F. Nagle and S. Tristram-Nagle, "Structure of Lipid Bilayers," *Biochimica et Biophysica Acta (BBA)—Reviews on Biomembranes* 1469 (2000): 159–195, https://doi.org/10.1016/S0304-4157(00)00016-2.

69. B. D. Almquist and N. A. Melosh, "Molecular Structure Influences the Stability of Membrane Penetrating Biointerfaces," *Nano Letters* 11 (2011): 2066–2070, https://doi.org/10.1021/nl200542m.

70. F. Otis, C. Racine-Berthiaume, and N. Voyer, "How Far Can a Sodium Ion Travel Within a Lipid Bilayer?," *Journal of the American Chemical Society* 133 (2011): 6481–6483, https://doi.org/10.1021/ja110336s.

71. C. Zhang, J. Tian, S. Qi, B. Yang, and Z. Dong, "Highly Efficient Exclusion of Alkali Metal Ions via Electrostatic Repulsion Inside Positively Charged Channels," *Nano Letters* 20 (2020): 3627–3632, https://doi.org/10.1021/acs.nanolett.0c00567.

72. Z.-J. Yan, Y.-W. Li, M. Yang, et al., "Voltage-Driven Flipping of Zwitterionic Artificial Channels in Lipid Bilayers to Rectify Ion Transport," *Journal of the American Chemical Society* 143 (2021): 11332–11336, https://doi.org/10.1021/jacs.1c06000.

73. D. Bassolino-Klimas, H. E. Alper, and T. R. Stouch, "Mechanism of Solute Diffusion Through Lipid Bilayer Membranes by Molecular Dynamics Simulation," *Journal of the American Chemical Society* 117 (1995): 4118–4129, https://doi.org/10.1021/ja00119a028.

74. H. S. Martin, K. A. Podolsky, and N. K. Devaraj, "Probing the Role of Chirality in Phospholipid Membranes," *ChemBioChem* 22 (2021): 3148–3157, https://doi.org/10.1002/cbic.202100232.

75. A. N. Thompson, I. Kim, T. D. Panosian, T. M. Iverson, T. W. Allen, and C. M. Nimigean, "Mechanism of Potassium-Channel Selectivity Revealed by Na^+ and Li^+ Binding Sites Within the KcsA Pore," *Nature Structural & Molecular Biology* 16 (2009): 1317–1324, https://doi.org/10.1038/nsmb.1703.

76. T. Dudev, K. Mazmanian, and C. Lim, "Competition Between Li^+ and Na^+ in Sodium Transporters and Receptors: Which Na^+ -Binding Sites are "Therapeutic" Li^+ Targets?," *Chemical Science* 9 (2018): 4093–4103, https://doi.org/10.1039/C7SC05284G.

77. S. Ahrari, T. N. Ozturk, and N. D'Avanzo, "Ion Behavior in the Selectivity Filter of HCN1 Channels," *Biophysical Journal* 121 (2022): 2206–2218, https://doi.org/10.1016/j.bpj.2022.04.024.

78. Y. K. Maeda, K. Kojima, T. Y. Nakamura, T. Nakatsu, and K. Irie, "Structure-Function Analysis of the Lithium-Ion Selectivity of the Voltage-Gated Sodium Channel," *Journal of General Physiology* 158 (2026): e202513855, https://doi.org/10.1085/jgp.202513855.

Supporting Information

Additional supporting information can be found online in the Supporting Information section.

Supporting File: anie73920-sup-0001-SuppMat.pdf.